

Received September 16, 2017, accepted October 30, 2017, date of publication November 3, 2017, date of current version December 22, 2017.

Digital Object Identifier 10.1109/ACCESS.2017.2769712

Flexible Positioning of Source-Detector Arrays in 3D Visualization Platform for Monte Carlo Simulation of Light Propagation

JINGJING GUO, ZHIGUO GUI, HONGHUA HOU, AND YU SHANG^{ID}

Key Laboratory of Instrumentation Science and Dynamic Measurement, North University of China, Taiyuan 030051, China

Corresponding author: Yu Shang (yushang@nuc.edu.cn)

This work was supported in part by the National Key Research and Development Program of China under Grant 2016YFC0101601, in part by the National Natural Science Foundation of China under Grant 61671413, and in part by the Shanxi Scholarship Council of China under Grant 2016-087.

ABSTRACT In current Monte Carlo (MC) simulations of the light propagation in biological tissues, the sources (S) or detectors (D) are mainly positioned in view of 2-D planes, leading to the rough accuracy, and low efficiency. This paper proposed a 3-D visualization platform with interactive view to determine the S–D coordinates as well as the incident direction of source light. Moreover, the proposed system permits implementation of the MC simulation in a flexible voxel spacing, beyond the original voxel of medical images. Validation studies on a realistic 3-D human head model show that the S–D pairs can be fast and accurately positioned on the tissue surface with assistance of the visualization platform, indicating its great potential for biomedical optical applications.

INDEX TERMS Monte Carlo simulation, light propagation, 3D visualization, source-detector arrays, NIRS.

I. INTRODUCTION

Monte Carlo (MC) simulation has become a widely used approach to describe the migrations of individual photons in turbid medium [1], particularly in biological tissues [2]–[4]. Within the turbid medium, the behavior of photon propagation in macroscale is termed as diffusive light [5]. Due to high accuracy in depicting various photon interactions with turbid medium, primarily, the absorption, scattering and refracting, MC simulation is often considered as a standard to evaluate other approaches investigating the diffusive light, such as analytical solutions or finite element approach for partial differential equation [6], [7]. MC simulation is conventionally utilized in near-infrared diffuse optical spectroscopy (NIRS) for validation and calibration of tissue absorption or oxygenation [8], [9], and more recently, adopted by us in blood flow measurement [10], [11]. An early open-source MC software package (MCML), which enables modeling of light propagation in multi-layered tissues, was proposed by Wang *et al.* [2] in 1990s. Following this pioneering work, more software packages based on triangle (TriMC3D [12] and MOSE [13]), tetrahedron (TIM-OS [4] and MMC [14]) or voxelized elements (tMCimg [3] or MCVM [8]), were developed by different groups, to realize light propagation simulation in heterogeneous tissues with arbitrary geometric boundary.

In the past, the use of MC simulation is limited by the computer capacity, as it involves a few time-consuming procedures, such as generating pseudo random number, making judgments of light transmitting, reflecting, scattering, or absorbing, as well as recording individual trajectory of a huge amount of photons [3], [8]. Moreover, the complex structure and tissue inhomogeneity greatly increase the computing time of MC simulations. Many efforts have been made to overcome this limitation, e.g., by optimization of MC codes with time-efficiency functions [15], by use of distributed computers [16], or far less costly, by implementation of compute unified device architecture (CUDA) platform on graphic processing units (GPUs) [17]–[21].

Currently, MC simulation is majorly adopted to quantify the distributions of light absorption or light intensity [8], [22]–[24], or to assist in optical imaging [25]. There exists a variety of factors that affect the accuracy of MC simulation, such as the values of absorption coefficient (μ_a), scattering coefficient (μ_s), anisotropy factor (g) and refractive index (n), as well as the geometry and structure in heterogeneous tissues. Additionally, MC simulation outcomes are influenced by the positioning of sources and detectors (S–D), specifically, the coordinates and incident directions at which the photons are injected and collected on the surface of

the tissue. In many applications of MC simulation, the sensors (i.e., S-D pairs) are conventionally positioned in two cross-view 2D planes (see example in Section 2.2), rather than in 3D visualization environment. The developments in NIRS make it possible to utilize light propagation data for resolving inverse problems, such as hemodynamic spectroscopy [10], [11] or imaging [6], [26], [27], and the image reconstruction needs a S-D array (i.e., a number of S-D pairs with specific alignment) to obtain sufficient measurements. In this situation, 2D-based positioning approaches, which localize the sources and detectors sequentially from two orthogonal views, substantially increase the laboring time when applied to S-D arrays. More importantly, the directions of light injections and collections, which are difficult to be determined in 2D views, are also the key factors affecting the light MC simulation results.

To the best of our knowledge, the S-D positioning (including locations and incident direction of light) in 3D environment for light MC simulation can only be found in commercial software such as TracePro[®]. However, those commercial softwares were designed to trace the light rays transmitting through discrete optical components, rather than expertise on biological tissues with continuous heterogeneity. To meet the increasing demands of light MC simulation for biomedical applications, it is essential to have a highly efficient way to position multiple S-D pairs with assistance of 3D visualization. Moreover, particular applications (e.g., image reconstruction) require the spatial unit of MC simulation (voxel or element) beyond the original voxel of medical images. In this study, a visualization platform was established by using an open-source C++ class library (i.e., The Visualization Toolkit-VTK), and it was integrated with a voxelized type of light MC simulation software (i.e., MCVM). With an interactive window, the visualization platform enables positioning the S-D array fast and accurately.

The proposed 3D visualization platform for S-D positioning was validated on a cube geometry and applied to a realistic human head model. For easy use in inverse problem of diffuse optics that requires minimized voxel (element) number, the visualization platform was adapted to permit MC simulation in a flexible voxel spacing. As a comparison of flexible spacing, the primary MC outcomes generated from original and enlarged voxel spacing were compared.

II. METHODS

A. CREATION OF VISUALIZATION PLATFORM WITH VTK

The 3D tissue models used for MC simulation are often reconstructed from medical images. As a generalized example, we selected a set of human head MRI images which had been well segmented into different tissue components (fat, muscle, skull, vessels, etc.) from a database that is public available (<http://brainweb.bic.mni.mcgill.ca/brainweb/>). A widely used open-source C++ class library for computer graphics and rendering, i.e., the Visualization Toolkit (VTK) version 7.0, was used to create visualization environment

as well as an interactive window. Among several available methods for surface or volume rendering, Marching Cubes algorithm was selected by us for 3D image reconstruction, owing to the excellent robustness, flexible parameterization and relative short processing time. Additionally, it is a voxel-based method, readily adaptable to voxelized type of MC software. The procedures for creating the 3D environment and positioning a source or detector are briefly described below:

- (i). Read the medical images or data set (in DICOM, JPEG or raw formats) by the function of 'vtkImageReader'.
- (ii). Preprocess the images and set a gray-value threshold of isosurface for use in Marching Cubes algorithm, and it is implemented by functions of 'vtkImageGaussianSmooth' and 'vtkImageThreshold'.
- (iii). Implement the Marching Cubes algorithm to generate the surface. First, we determined the cubes (voxels) intersecting the isosurface in the 3D data field, according to the gray-value threshold. There are a total of 15 cases in the intersection relations between the isosurface and each cube. Then, the intersections are connected to triangles or polygons via a simple linear interpolation. Next, normal direction of triangles or polygons is obtained so that isosurface images are displayed. The step is mainly implemented by function of 'vtkMarchingCubes'. Additionally, some other functions, such as 'vtkPolyDataMapper', 'vtkActor', 'vtkRenderer' and 'vtkRenderWindow', are involved in process for rendering and visualization.
- (iv). Under the assistance of visualization, we created an interactive window and obtained the direction of incident light by use of widget 'vtkPlaneWidget' in VTK library, which permits cutting the 3D model in slice at any angle. Because the angle of the slice cutting can be adjusted arbitrarily, we can further get the tangent plane of the light source or detector, from which the normal direction can be obtained. Moreover, coordinates of the source or detector can also be displayed through picking them by mouse in visualization panel, using customer-amended class of 'LeftButtonDown'.

B. POSITIONING OF SOURCE-DETECTOR PAIRS IN VISUALIZATION PLATFORM

The above methodologies were evaluated on a cube model with known coordinates and directions. As shown in Figure 1, the coordinate and the normal direction that were selected at origin point along vertical axis, via 3D visualization platform, are (0.00, 0.00, 0.01) and (-0.00, 0.03, 1.00) respectively, which are highly consistent with the true values, i.e., (0, 0, 0) and (0, 0, 1) respectively. This evaluation verifies that the proposed visualization tool is highly precise in positioning the light sources and detectors.

For biomedical application, the photon migrations were often traced on real tissues or organs characterized by medical images such as CT or MRI. Here we compared the 3D approach described above (i.e., procedures (i)-(iv)) with the conventional 2D cross-view approach in positioning a

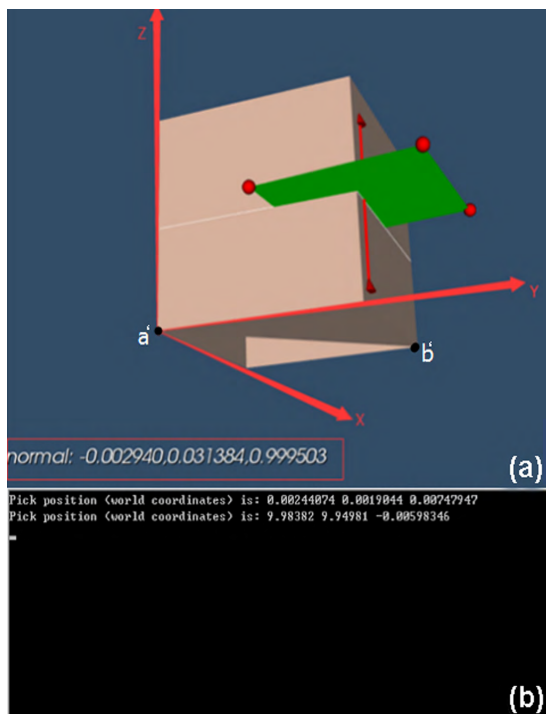


FIGURE 1. The coordinates (b) and normal direction (a) of the selected point on cube, determined by visualization platform and interactive window. The selected point represents either a source or a detector.

sensor (source or detector) from the same set of head MRI images (after segment). The target sensor position is 20mm above the left eyebrow. With 2D cross-view approach, one pair of 2D coordinate is firstly determined in the coronal plane (i.e., X-Z tangent plane) through manual or automatic selection of the pixel, with assistance of the calculation from distance and slice spacing (see Figure 2a). Then, another pair of 2D coordinate is determined in transverse plane (i.e., X-Y tangent plane) by similar procedure (see Figure 2b). Here the coronal and transverse planes form a cross-view pair, and the 3D coordinates are ultimately determined by combination of two pairs of 2D coordinates (see Figure 2b). By contrast, the 3D coordinates are one-time determined by our proposed approach in 3D platform (Figure 2c). Furthermore, the normal direction of incident light, which could only be roughly estimated in 2D cross-view approach, is readily and accurately determined in 3D view (Figure 2c).

Table 1 lists the comparisons of 2D cross-view and 3D approach in positioning the S-D sensors. As a brief summary, the 3D approach enables fast and accurate S-D setup for light MC simulation.

C. INTEGRATION OF VISUALIZATION PLATFORM WITH VOXELIZED MC SOFTWARE

To best use the function of visualization, substantially amends were made to the programming codes of a voxelized type of MC software (i.e., MCVm) [8]. Specifically, the coordinates of both sources and detectors were written in form of arrays into the MC input file. Correspondingly, only the photons having escaped at detector arrays were recorded in the MC

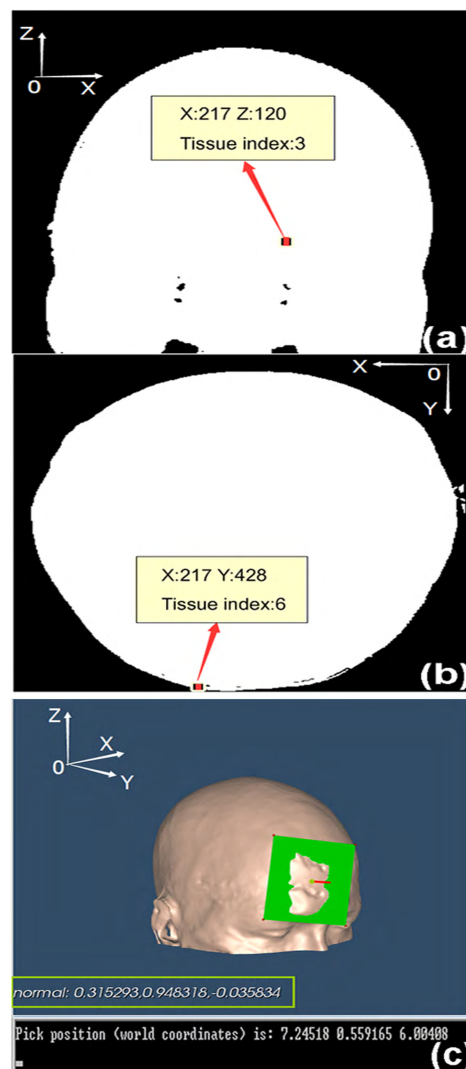


FIGURE 2. Comparison of 2D cross-view and 3D approach in positioning a source or detector.(a) one pair of 2D coordinate is determined in the coronal plane (i.e. the X-Z tangent plane; $X,Z = (217, 120)$; pixel spacing = 0.05 cm; so the 2D coordinate is (10.85, 6.00) cm; (b) another pair of 2D coordinate is determined in the transverse plane (i.e., the X-Y tangent plane; $X,Y = (217, 428)$; pixel spacing = 0.05 cm; so the 2D coordinate is (10.85, 21.40) cm; thus the 3D coordinate is obtained as (10.85, 21.40, 6.00) cm; (c) the 3D coordinate is one-time determined in 3D view by our proposed approach, to read as (7.25, 0.56, 6.00) cm. Note that the origin of coordinate in 3D view is different from that in 2D view, and there is a coordinate conversion between two views (i.e., subtracting coordinates from the head size in x axis (18.1 cm) and in y axis (21.7 cm), respectively; while remaining coordinate unchanged in z axis). As such, the ultimate coordinates converting from 3D to 2D views are also (10.85, 21.40, 6.00) cm. Besides, the norm direction of incident light is also accurately determined, to read as (0.32, 0.95, -0.03).

output file, rather than that all escaping photons in original MCVm codes were recorded. The amends greatly save the storing space as well as the thereafter time to read the data in output file.

D. REGISTRATION OF THE MC OUTCOMES WITH TISSUE IMAGES

For an optical setup, the outcomes of light MC simulation only distribute within a portion of volume covered by the

TABLE 1. Comparisons between 2D cross-view and 3D approach in term of procedures or functions for positioning sources and detectors.

Procedures/functions	2D cross-view	3D approach
Utilized data	Two medical slices manually selected in orthogonal directions	A dataset of medical slices
Specialized tool	No requirement	Programming in VTK
Procedures to determine S-D coordinates	Determine 2D coordinates respectively in two slices, then combine into 3D coordinates	Determine 3D coordinates directly in visualization platform
Source directions	Estimate the 3D directions from two 2D slices	Determine 3D directions directly in visualization platform
Accuracy	roughly	precisely
Time of processing	minutes	seconds

S-D pairs. This volume needs to be visibly localized in the whole head for displaying the MC outcome. Below are the procedures to map the MC outcomes into the original MRI images (i.e., tissue images see 2D and 3D view in Figure 4a and Figure 4d respectively). First, a small value of the optical parameter (e.g., light absorption or photon path length) was set as the threshold for all slices to gate the lower values of MC outcomes into zeros. After this step the outline of MC outcome (e.g., tissue absorption) was clearly visible (see 2D and 3D view in Figure 4b and Figure 4e respectively). This threshold value was used to represent the inside of tissue. Then, another value, which is slightly below the threshold, was used to represent the outside (including the edges) of tissue. Each pixel values in the original MRI slice was replaced by one of the two different values according to the category (i.e., inside or outside of tissue). This two-value image provided the outline image of tissue (see 2D and 3D view of Figure 4c and Figure 4f respectively). Both the MC simulation image and the two-value tissue image were registered into the same slice according to their coordinates, and either of the two values was adopted only when the pixel value is zero in MC simulation image. Figure 4c and Figure 4f show the final result of registration in 2D and 3D views respectively.

E. FLEXIBLE ELEMENT SPACING IN MC SETUP

In the inverse problems (e.g., diffuse optical imaging) wherein the light propagation information is needed but the physical S-D pairs are few (limited by the instrument cost and data acquisition time), reducing the number of voxels (also refers to as the ‘elements’ in some literature) is of great benefits for accurate reconstruction of anomaly contrasts from the limited S-D measurements. To meet this demand, the 3D visualization platform was designed with a function

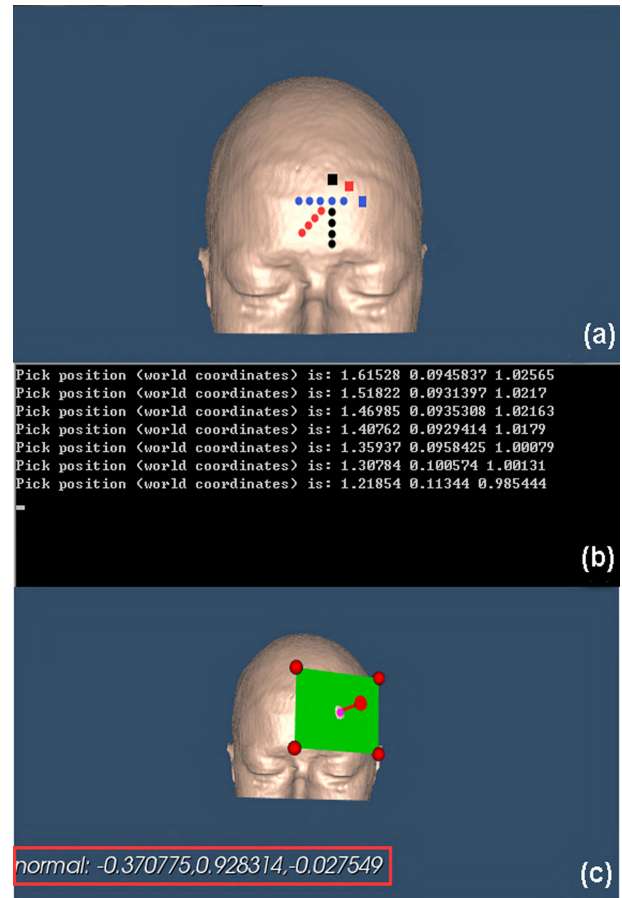


FIGURE 3. 3D human head reconstructed by VTK from MRI data; (a) positioning of 3 sources (denoted with squares: source 1 (blue), source 2 (black) and source 3 (red)) and 15 detectors (denoted with circles, a group of 5 detectors corresponds to each source, with separations in range of 1.0 to 3.0 cm); (b) the coordinates of the selected sources and detectors; (c) the incident light direction from one source via interactive graphics.

of distance measurement to conveniently resize the voxels at preferred spacing.

As an example, we performed the MC simulations on a part of human head covered by the S-D arrays with the selected coarse voxels ($45 \times 30 \times 30$) at the enlarged spacing (0.2 cm). The primary outcomes, including the photon absorption and path length, were compared with those performed on the complete head with fine voxels ($362 \times 362 \times 434$) at original spacing (0.05 cm). For both types of voxels, the optical parameters were set as: absorption coefficient $\mu_a = 0.06 \text{ cm}^{-1}$, scattering coefficient $\mu_s = 80 \text{ cm}^{-1}$, anisotropy factor $g = 0.9$, and refractive index $n = 1.37$. From each of the three sources, a total of 10 million photon packets were injected into the tissue, and the escaping photons were collected by 5 detectors.

III. RESULTS

A. THREE DIMENSIONAL VISUALIZATION AND POSITIONING OF S-D PAIRS ON HUMAN HEAD

Figure 3 shows the 3D human head reconstructed by VTK from MRI data, following steps (i) to (iv). Figure 3a exhibits

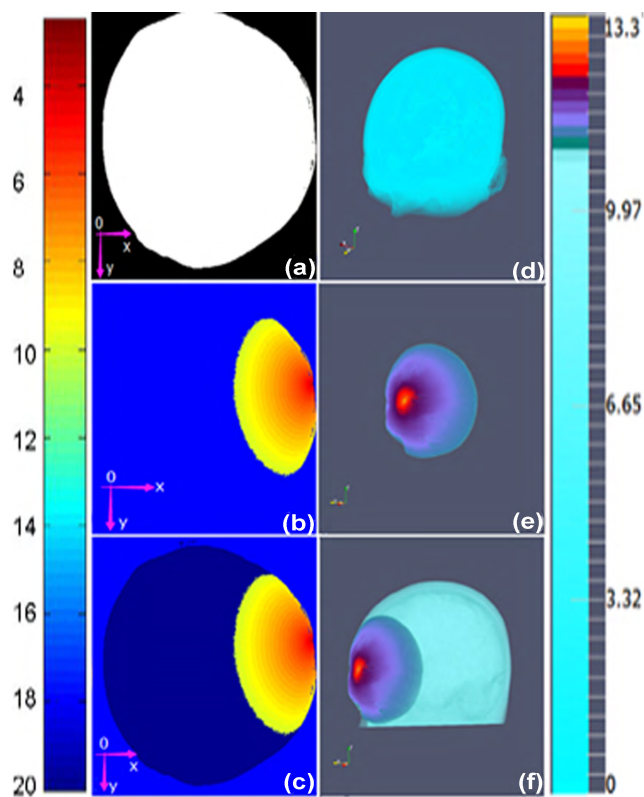


FIGURE 4. The original MRI images (a and d); the light MC simulation outcomes (light absorption, in arbitrary unit) without (b and e) and with (c and f) registration to the MRI head image. The outcomes are illustrated in 2D (a, b and c) and 3D (d, e and f) views respectively.

the placement of a 3×5 S-D array on the head surface. The coordinates of 3 sources and 15 detectors via 3D visualization platform are shown in Figure 3b. For clear demonstration, the interactive graphics to determine an incident light direction is illustrated in Figure 3c.

With use of the amended MC codes and performed by a Lenovo ThinkCentre M8600t computer (3.4 GHz CPU and 16 GB physical memory), the average storage disk and analysis time for all detected photons in a S-D pair were 6.4 MB and 0.1 second, sharply dropped to 9.6% and 1.39% respectively, when compared with 665 MB and 7.2 seconds by using the original MC codes.

With the assistance of 3D visualization platform and interactive window to position the S-D array, the accuracy of S-D configuration is visibly ensured, and S-D setup time is remarkably reduced. Furthermore, with use of the selected head part, coarse voxels and the amended MC codes, the voxel number, output file size, and data analysis time were further dropped to 0.07%, 0.07% and 2.6% respectively, when compared with the outcomes using complete head, fine voxels and the original MC codes.

B. REGISTRATION OF THE LIGHT MC SIMULATION OUTCOMES INTO 2D AND 3D VIEWS

Figure 4 illustrates the distributions of light MC outcomes (represented by the light absorption) without (b and e)

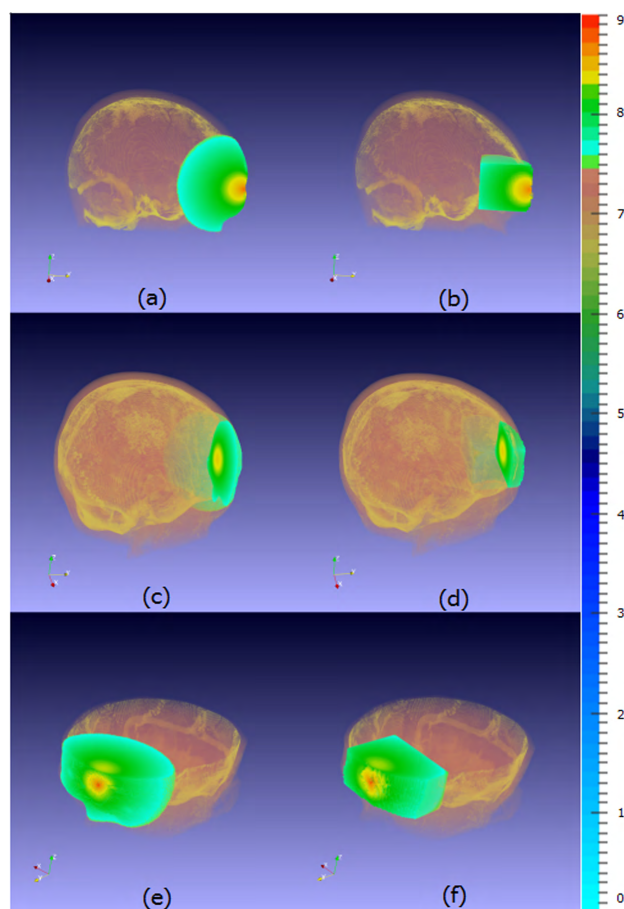


FIGURE 5. Distributions of tissue absorption generated by fine (a) (c) (e) and coarse (b) (d) (f) voxels respectively. From top to bottom: sagittal, coronal and transverse section.

and with (c and f) registration to the original MRI images (a and d), presented in both 2D (a, b and c) and 3D views (d, e and f). It can be seen that the light MC simulation only distributes in a portion of volume covered by the S-D pairs (b and e). With registration to the tissue images that provides the head outline, the MC outcomes are clearly localized (c and f).

C. TISSUE ABSORPTION

Tissue absorption is a parameter often used to indicate how much the photon weight from the light source is kept within tissue. Figure 5 shows the distribution of tissue absorption from a representative S-D pair (after registration with MRI image), exhibited in sagittal (a and b), coronal (c and d) and transverse planes (e and f). Note that an open-source software ParaView (Kitware, NY, USA) was utilized to optimize the contrast rendering for visualization in Figure 4 and Figure 5. For comparison, the tissue absorption distributions generated by fine (0.05 cm) and coarse (0.2 cm) voxels are displayed in the Figure 5(a),(c),(e) and Figure 5(b),(d),(f), respectively. Here, the complete head data set consists of fine voxels in size of $362 \times 362 \times 434$. A part was taken from the complete head and resized with coarse voxels of $45 \times 30 \times 30$. As expected,

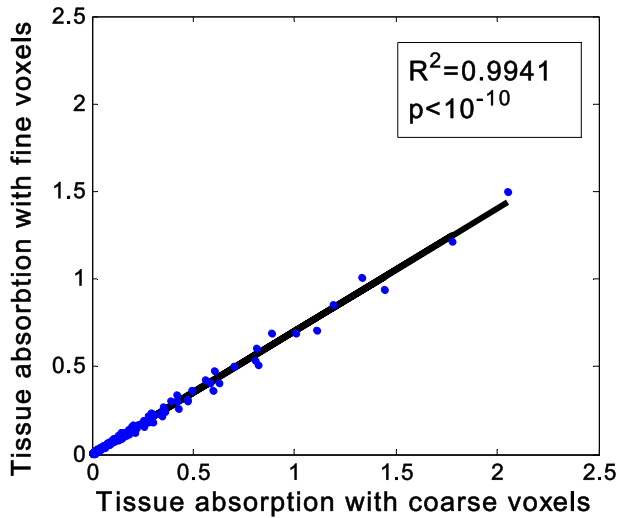


FIGURE 6. Regression analysis between the TTA generated by fine and coarse voxels. Note that the unit of TTA is arbitrary, dependent on the number of photon packets injected from the source.

the tissue absorption concentrates highly around the light source, and its concentration declines with the increase of the distance between the source and voxel. Both the fine and coarse voxels are found to generate similar patterns in tissue absorption distribution, and the global difference (i.e., the difference averaging over the overlapped volume) is 8.30%.

For a complete comparison, we calculated the total tissue absorption (TTA), which was defined as the sum of the tissue absorptions generated by all of the three sources. The comparison between fine and coarse voxels was quantified through regression analysis of the TTA in overlapped regions. As shown in Figure 6, an excellent linear relationship between the two TTA was found ($R^2 = 0.99$, $p < 10^{-10}$), confirming the similarity between fine and coarse voxels in the MC outcomes.

D. PHOTON PATH LENGTH

Photon path length (PPL) is a parameter quantifying how long distance the photons travel through a S-D pair. Generally, the photon counts decline with the increase in PPL, and this relation is affected by the tissue geometry and heterogeneity. As shown in Figure 7, the PPL generated from fine and coarse voxels in a representative S-D pair (Source 1 and Detector 2) exhibits a close distribution pattern in photon counts, with 8.10% in difference.

Apart from the representative S-D pair, the difference between fine and coarse voxels was calculated for each of 15 S-D pairs. Figure 8 shows the PPL differences in all S-D pairs, in which the detector is numbered according to the distance to the source (i.e., from 1.0 to 3.0 cm). Generally, the difference increases when the detector is away from the source, and the difference is mostly no larger than 15%. The averaging PPL difference over all S-D pairs is 10.23%. Considering the sharply decreased voxel number (only 1.6% of the fine voxels) that is great beneficial for inverse problem,

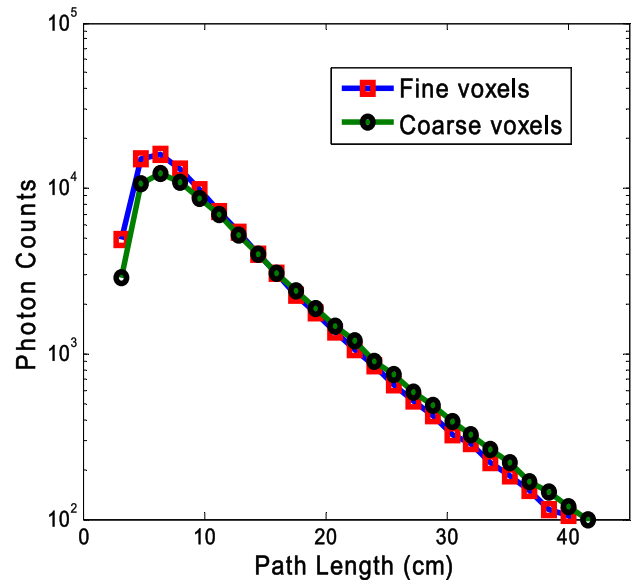


FIGURE 7. The relation between photon counts and path length in a representative S-D pair.

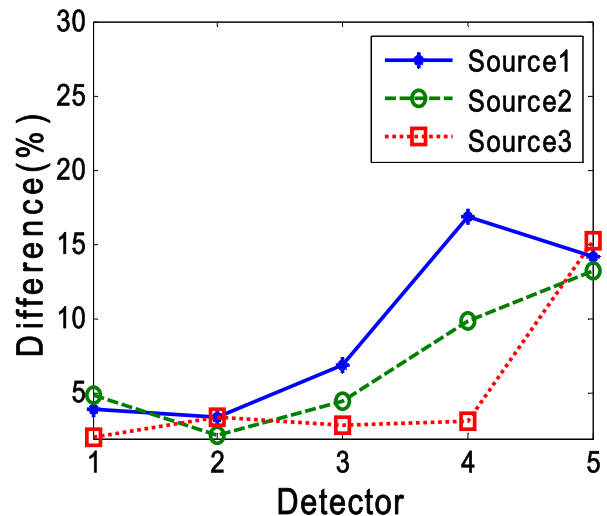


FIGURE 8. The difference between fine and coarse voxels in PPL (%) for each S-D pair.

the coarse voxels are useful for some practical applications such as optical image reconstruction.

IV. DISCUSSION AND CONCLUSIONS

Proper localization of source and detector is critical for precise simulation of the light propagation within the biological tissue. In most of MC simulations, the sources and detectors are mainly positioned in view of 2D planes, leading to the rough accuracy and low efficiency. Additionally, approach to flexibly resize the voxel (or element) is required for particular applications (e.g., image reconstruction). To this end, no specific approaches on how to accurately position the S-D pairs or flexible spacing for MC simulation were found in literature. This study presents a 3D visualization platform

with interactive windows to determine the coordinates and directions of S-D pairs. Moreover, the system permits implementation of the MC simulation in a flexible voxel spacing, which is of great benefit for inverse problems in diffuse optics.

For a target tissue characterized by medical images, the algorithm of Marching Cubes was utilized to render the iso-surface and provide 3D visualization via the VTK tool. The 3D visualization platform, along with an interactive window, allows users to sequentially position S-D pairs, from which the coordinates and directions of each source or detector were determined.

The accuracy of the proposed approach was validated on a cube model with known coordinates and directions, and it was applied to MRI images of a human head. Highly efficient way in positioning of 3×5 S-D pairs was implemented owing to the assistance of 3D visualization platform. The derived information of coordinates and directions on fine and coarse voxels was used, respectively, as input parameters for light propagation simulations. To accommodate the merits of 3D visualization platform, the programming codes of conventional voxelized MC software (i.e., MCVM) were amended to reduce the storage space and data analysis time.

The results show that the combination of 3D visualization platform and MC software has the capacity to timely and precisely perform light propagation simulations with flexible voxel spacing. The type of coarse voxels was found to generate the distribution of photon absorptions and path lengths similar to those generated by fine voxels, while preserving minimal voxel number (only 1.6% of the original voxels in this study) which is beneficial for inverse problems.

To conclude, a 3D visualization platform was developed in this study for convenient use of MC software, which is conventionally set up in 2D views. With assistance of 3D views and the interactive window, we realized fast and precise positioning of S-D arrays on realistic human head. Although the proposed platform was applied to a representative voxelized MC software (i.e., MCVM) in this study, the involved methodologies can be readily adaptable to other open-source MC software. Studies are being carried out to perform fast light propagation simulation for a large S-D array over heterogeneous tissue and used for inverse problems of optical imaging.

CONFLICTS OF INTEREST

The authors declare no conflict of interest.

REFERENCES

- [1] J. Colombi and K. Louedec, "Monte Carlo simulation of light scattering in the atmosphere and effect of atmospheric aerosols on the point spread function," *J. Opt. Soc. Amer. A*, vol. 30, no. 11, pp. 2244–2252, Nov. 2013.
- [2] L. Wang, S. L. Jacques, and L. Zheng, "MCML—Monte Carlo modeling of light transport in multi-layered tissues," *Comput. Methods Programs Biomed.*, vol. 47, pp. 131–146, Jul. 1995.
- [3] D. A. Boas, J. P. Culver, J. J. Stott, and A. K. Dunn, "Three dimensional Monte Carlo code for photon migration through complex heterogeneous media including the adult human head," *Opt. Exp.*, vol. 10, no. 3, pp. 159–170, Feb. 2002.
- [4] H. Shen and G. Wang, "A tetrahedron-based inhomogeneous Monte Carlo optical simulator," *Phys. Med. Biol.*, vol. 55, no. 4, pp. 947–962, Feb. 2010.
- [5] W. B. Baker, A. B. Parthasarathy, D. R. Busch, R. C. Mesquita, J. H. Greenberg, and A. G. Yodh, "Modified Beer-Lambert law for blood flow," *Biomed. Opt. Exp.*, vol. 5, no. 11, pp. 4053–4075, Nov. 2014.
- [6] H. Dehghani et al., "Near infrared optical tomography using NIRFAST: Algorithm for numerical model and image reconstruction," *Commun. Numer. Methods Eng.*, vol. 25, pp. 711–732, Jun. 2009.
- [7] S. R. Arridge and J. C. Hebden, "Optical imaging in medicine: II. Modelling and reconstruction," *Phys. Med. Biol.*, vol. 42, no. 5, pp. 841–853, May 1997.
- [8] T. Li, H. Gong, and Q. Luo, "MCVM: Monte Carlo modeling of photon migration in voxelized media," *J. Innov. Opt. Health Sci.*, vol. 3, pp. 91–102, Apr. 2010.
- [9] T. Li et al., "Simultaneous measurement of deep tissue blood flow and oxygenation using noncontact diffuse correlation spectroscopy flow-oximeter," *Sci. Rep.*, vol. 3, p. 1358, Feb. 2013.
- [10] Y. Shang, T. Li, L. Chen, Y. Lin, M. Toborek, and G. Yu, "Extraction of diffuse correlation spectroscopy flow index by integration of N th-order linear model with Monte Carlo simulation," *Appl. Phys. Lett.*, vol. 104, no. 19, p. 193703, May 2014.
- [11] Y. Shang and G. Yu, "A N th-order linear algorithm for extracting diffuse correlation spectroscopy blood flow indices in heterogeneous tissues," *Appl. Phys. Lett.*, vol. 105, no. 13, p. 133702, Sep. 2014.
- [12] E. Margallo-Balbas and P. J. French, "Shape based Monte Carlo code for light transport in complex heterogeneous tissues," *Opt. Exp.*, vol. 15, pp. 14086–14098, Oct. 2007.
- [13] S. H. Ren et al., "Molecular optical simulation environment (MOSE): A platform for the simulation of light propagation in turbid media," *PLoS ONE*, vol. 8, p. 0061304, Apr. 2013.
- [14] Q. Fang, "Mesh-based Monte Carlo method using fast ray-tracing in Plücker coordinates," *Biomed. Opt. Exp.*, vol. 1, no. 1, pp. 165–175, Aug. 2010.
- [15] N. S. Zolek, A. Liebert, and R. Maniewski, "Optimization of the Monte Carlo code for modeling of photon migration in tissue," *Comput. Methods Programs Biomed.*, vol. 84, pp. 50–57, Oct. 2006.
- [16] A. J. Page, S. Coyle, T. M. Keane, T. J. Naughton, C. Markham, and A. Ward, "Distributed Monte Carlo simulation of light transportation in tissue," in *Proc. Int. Parallel Distrib. Process. Symp.*, Apr. 2006, pp. 235–238.
- [17] N. Ren, J. Liang, X. Qu, J. Li, B. Lu, and J. Tian, "GPU-based Monte Carlo simulation for light propagation in complex heterogeneous tissues," *Opt. Exp.*, vol. 18, no. 7, pp. 6811–6823, Mar. 2010.
- [18] C. Jiang, H. He, P. C. Li, and Q. M. Luo, "Graphics processing unit cluster accelerated Monte Carlo simulation of photon transport in multi-layered tissues," *J. Innov. Opt. Health Sci.*, vol. 5, p. 1250004, Apr. 2012.
- [19] E. Alerstam, W. C. Lo, T. D. Han, J. Rose, S. Andersson-Engels, and L. Lilje, "Next-generation acceleration and code optimization for light transport in turbid media using GPUs," *Biomed. Opt. Exp.*, vol. 1, pp. 658–675, Sep. 2010.
- [20] Q. Q. Fang and D. A. Boas, "Monte Carlo simulation of photon migration in 3D turbid media accelerated by graphics processing units," *Opt. Exp.*, vol. 17, no. 22, pp. 20178–20190, Oct. 2009.
- [21] O. W. Yang and B. Choi, "Accelerated rescaling of single Monte Carlo simulation runs with the graphics processing unit (GPU)," *Biomed. Opt. Exp.*, vol. 4, pp. 2667–2672, Nov. 2013.
- [22] D. Tendeiro, G. Lopes, P. Vieira, and J. P. Santos, "Monte Carlo simulation of laser beams interaction with the human eye using geant4," *Biomed. Eng. Online*, vol. 13, p. 58, May 2014.
- [23] K. Peng et al., "Study on photon transport problem based on the platform of molecular optical simulation environment," *J. Biomed. Imag.*, vol. 2010, p. 913434, Jan. 2010.
- [24] Y. Guo and J. L. Tan, "Monte Carlo simulation of retinal light absorption by infants," *J. Opt. Soc. Amer. A*, vol. 32, pp. 271–276, Feb. 2015.
- [25] A. E. Cerussi, N. Mishra, J. You, N. Bhandarkar, and B. Wong, "Monte Carlo modeling of light propagation in the human head for applications in sinus imaging," *J. Biomed. Opt.*, vol. 20, p. 035004, Mar. 2015.
- [26] M. Schweiger and S. Arridge, "The Toast plus software suite for forward and inverse modeling in optical tomography," *J. Biomed. Opt.*, vol. 19, p. 040801, Apr. 2014.
- [27] A. T. Eggebrecht et al., "Mapping distributed brain function and networks with diffuse optical tomography," *Nature Photon.*, vol. 8, pp. 448–454, Jun. 2014.



JINGJING GUO received the B.S. degree in biomedical engineering from the North University of China, Taiyuan, China, in 2015, where she is currently pursuing the M.S. degree in biomedical engineering. Her research interests include image reconstruction and three-dimensional visualization.



HONGHUA HOU received the B.S. degree in electrical engineering and the M.S. degree in signal processing from the North University of China. She is currently an Associate Professor with the North University of China. Her research interests include signal processing, medical image processing, and computer vision.



ZHIGUO GUI received the B.S. degree in electrical engineering, the M.S. and Ph.D. degrees in signal processing from the North University of China. He was a Post-Doctoral Researcher with the Southeast University, China. He is currently a Full Professor with the North University of China. His research interests include image reconstruction, image processing, and signal processing.



YU SHANG received the B.S. degree in applied mathematics and the M.S. degree in biomedical engineering from Jilin University, China, in 1999 and 2004, respectively, and the Ph.D. degree in biomedical engineering from Tsinghua University, China, in 2008. He was a Post-Doctoral Scholar/Fellow from 2008 to 2013 and a Research Scientist with the University of Kentucky, USA, from 2013 to 2015. He is currently a Full Professor with the North University of China. His research interests include image reconstruction, biomedical optical spectroscopy, and tomography.

...